ADVANCED FUNCTIONAL MATERIALS
www.afm-journal.de

Materials Views
www.MaterialsViews.com

Electrical Transport and Oxygen Exchange in the Superoxides of Potassium, Rubidium, and Cesium

Oliver Gerbig, Rotraut Merkle, and Joachim Maier*

Dedicated to Professor Arndt Simon on the occasion of his 75th birthday

Conductivity, ionic transference number, and chemical diffusion coefficients are determined for KO_2, RbO_2, and CsO_2. Based on such results, a defect-chemical model is constructed. These superoxides are found to exhibit a total conductivity in the range of 3×10^{-7} to 5×10^{-5} S cm^{-1} at 200 °C with contributions from ionic and electronic carriers. The ionic conductivity is caused by alkali interstitials and superoxide vacancies as mobile defects, and is found to exceed the n-type electronic conductivity. ^{18}O isotope exchange on powder samples (monitoring the gas phase composition) shows that essentially all oxygen can be exchanged. At high pO_2 this largely occurs without breaking of the O–O bond—indicating a sufficient mobility of molecular superoxide species in the solid—and with an effective rate constant that is much higher than for other large-bandgap mixed conducting materials such as $SrTiO_3$.

1. Introduction

Alkali oxygen batteries with nonaqueous electrolytes involve formation and decomposition of alkali peroxide or superoxide at the positive electrode according to $nM^+ + O_2 + ne^- \rightleftharpoons M_nO_2$. The lithium–oxygen battery (with M = Li and $n = 2$) yields the highest theoretical specific energy density of these electrochemical energy storage systems, but also high overpotentials upon charging and discharging the cell (see, e.g., refs[1–6]). In this context several theoretical studies of the thermodynamics[7–13] and transport and reaction kinetics[14–23] in lithium peroxide were conducted. The transport properties of Li_2O_2 were experimentally first investigated in ref.[24] by impedance spectroscopy combined with DC measurements utilizing selectively blocking electrodes, and more recently in ref.[25] using impedance and NMR. According to this, Li_2O_2 was found to be a mixed conductor with lithium vacancies and holes (localized on peroxide ions yielding superoxide species) as main charge carriers, whereby owing to predominating ionic disorder the ionic conductivity exceeds the electronic conductivity. The kinetic limitations of the lithium oxygen battery can largely be overcome for heavier alkali metals such as Na, which in carbonate or ether electrolytes preferably forms superoxides,[26,27] and for which an increased solubility is thought to contribute to faster reaction. Recently, also a potassium–oxygen battery with formation of KO_2 as discharge product was investigated.[28]

Notwithstanding the enormous technological driving force for studying charge carriers in these materials, exploration of defect chemistry of the superoxides is of substantial fundamental interest because of the expected peculiarities. In general, the heavier the alkali metal, the higher—under ambient conditions—the thermal stability of the superoxides when compared to the respective peroxides. Here we concentrate on those alkali metals for which the superoxide is the thermodynamically stable metal–oxygen phase under standard conditions. For sodium at ambient temperature and 1 bar O_2, the thermodynamically stable phase is the peroxide Na_2O_2, and the stability of Na_2O_2 over NaO_2 further increases with increasing temperature.[29] Sodium superoxide may form in Na–O batteries at room temperature for kinetic reasons (see, e.g., refs.[26,27,30]) and is predicted to become the stable phase for particles smaller than about 10 nm based on ab initio calculations.[31] An upcoming publication from our group will deal with the defect chemistry of sodium peroxide; it is worth to mention that its electronic conductivity is found to be p-type as in Li_2O_2.[32]

In case of potassium, one can switch between superoxide and peroxide phases by adjusting temperature and oxygen partial pressure pO_2 (with high pO_2 and lower T favoring the superoxide).[33] For Rb and Cs, superoxide is the dominating oxygen-containing phase over a rather extended range of conditions.[34] The electrical transport properties and the reaction kinetics in alkali superoxides are essentially terra incognita. It is of practical importance as well as of high fundamental interest to gain a detailed insight in the defect chemistry and the transport properties of these materials, in particular to understand the trends with increasing atomic number of the alkali metal, and to elaborate similarities (such as ionic defects types) and differences (nature of electronic defects) between the alkali peroxides and superoxides. Recently, the alkali superoxides were also paid attention to in view of low temperature spin ordering effects.[35–37] Nevertheless, their electrical properties and defect chemistry were only scarcely investigated so far.

In the present publication we identify the majority ionic and electronic carriers in K-, Rb- and Cs-superoxides based on measurements of pO_2-dependent conductivity and electromotive force (EMF). Additional information on mobile oxygen defects is obtained from ^{18}O isotope exchange. On the basis of these results a defect chemical model is set up.

Dr. O. Gerbig, Dr. R. Merkle, Prof. J. Maier
Max Planck Institute for Solid State Research
Heisenbergstr. 1, 70569 Stuttgart, Germany
E-mail: r.merkle@fkf.mpg.de

DOI: 10.1002/adfm.201404197

© 2015 WILEY-VCH Verlag GmbH & Co. KGaA, Weinheim

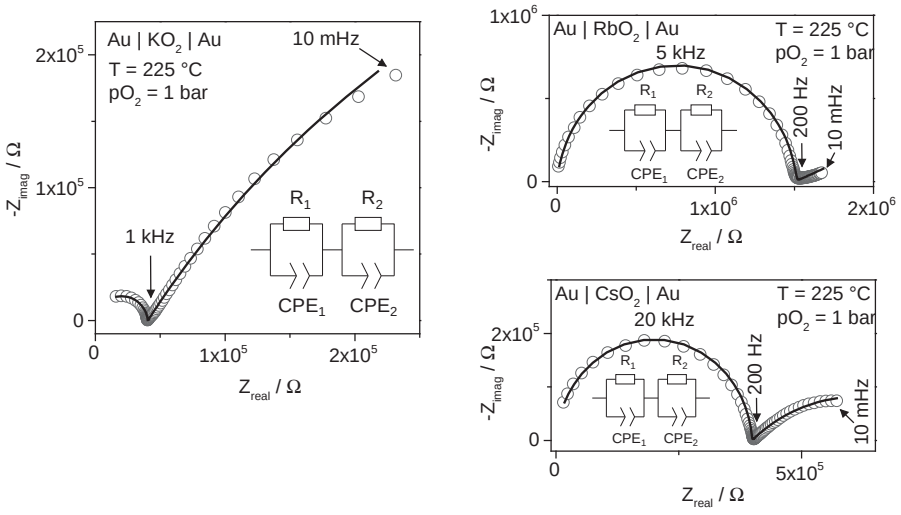

Figure 1. Electrochemical impedance spectra of the cells Au | KO_2 | Au, Au | RbO_2 | Au, and Au | CsO_2 | Au at 225 °C and 1 bar pO_2, insets show the equivalent circuits used for fitting and the solid line is the fit result.

2. Results and Discussion

2.1. Electrochemical Characterization

The electrochemical impedance spectra of Au|MO_2|Au (M = K, Rb, Cs) cells are characterized by two relaxation processes, each of which can be fitted by a resistor and a constant phase element (CPE, nonideality parameter typically 0.9–0.95) in parallel (**Figure 1**). According to the capacitances (calculated from the fitting parameters of the CPE[38]), the high frequency semicircles can unambiguously be assigned to the bulk response (with ε_r (KO_2) = 29, ε_r (RbO_2) = 15, and ε_r (CsO_2) = 13), while the low frequency relaxation process originates from the blocking of ionic charge carriers at the gold electrodes. The spectra contain no evidence for current constriction caused by poor grain contacts in the cold pressed samples, which is in accordance with the high density of the pellets (>95% of the theoretical density) and high plastic deformation of the grains already upon cold pressing. In spectra measured at 250 °C, a further contribution at mid frequencies appears for RbO_2 and CsO_2 with gold electrodes after some time. The capacitance of the relaxation process (C ≈ 10^{-9}–10^{-8} F) is in a range typical for blocking grain boundaries. However, since the contribution develops only after extended exposure to high *T*, it is likely caused by a blocking layer formed by reaction of the superoxides with the gold electrodes. Although gold is thermodynamically stable against oxidation by molecular oxygen at ambient pressures even at high temperatures, it can react to ternary oxides with alkali superoxides and peroxides at moderate temperatures.[39]

The temperature dependences of the total (ionic + electronic) bulk conductivity of as-prepared KO_2, annealed KO_2, RbO_2, and CsO_2 in 10^{-5} or 10^{-4} bar pO_2 and 1 bar pO_2 are shown in **Figure 2**. Apart from RbO_2 at low *T*, the conductivities of all three superoxides are quite similar; for given pO_2 and *T* they lie within one order of magnitude. The activation energies and their changes depending on conditions will be discussed in the context of a defect chemical model at the end of this

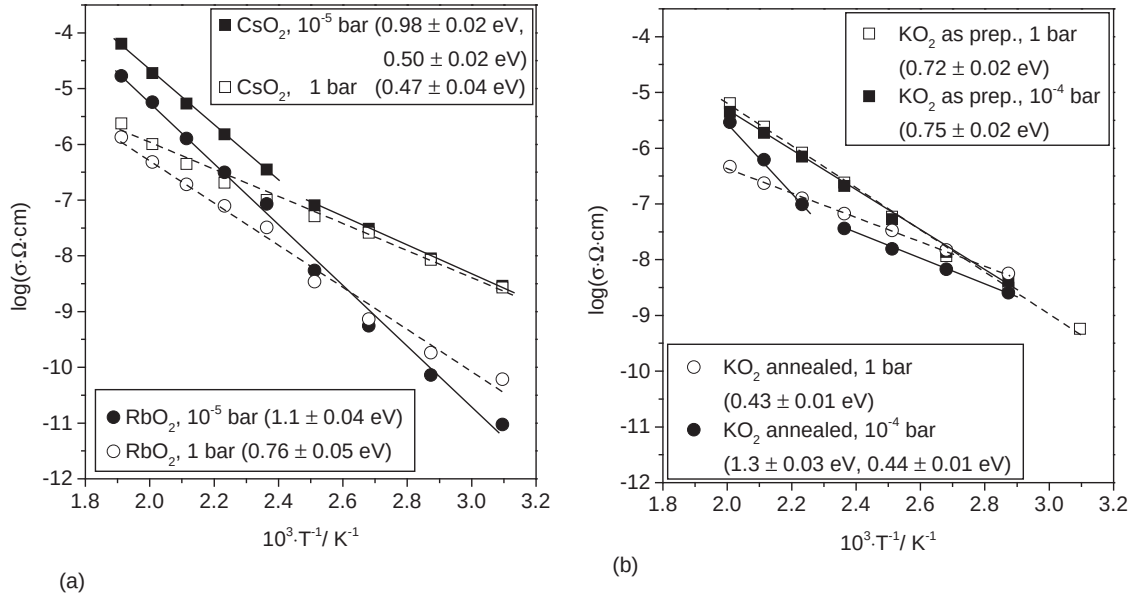

Figure 2. Temperature dependence of the total bulk conductivity of a) CsO_2 at 1 bar pO_2 (open squares) and 10^{-5} bar pO_2 (solid squares) and of RbO_2 at 1 bar pO_2 (open circles) and 10^{-5} bar pO_2 (solid circles); b) of as-prepared KO_2 at 1 bar pO_2 (open squares) and 10^{-4} bar (solid squares) as well as of annealed KO_2 at 1 bar pO_2 (open circles) at 10^{-4} bar pO_2 (solid circles). The activation energies are given in brackets.

© 2015 WILEY-VCH Verlag GmbH & Co. KGaA, Weinheim

section. It is interesting to note that the total conductivities of the K-, Rb-, and Cs-superoxides are in the same range as the total (predominantly ionic) conductivity found for Li_2O_2 in ref.[24] On the other hand, we have to state that the extremely high room temperature electronic conductivity of KO_2 of >10 Ω^{-1} cm^{-1} reported in ref.[40] cannot be confirmed. The electrical resistance of the cell Au | KO_2 | Au at 25 °C is even beyond the measurement limit of an electrometer with >100 GΩ input resistance. The value of the electronic conductivity could not be exactly determined in the present investigation (cf. discussion of EMF results below) but is certainly ≤10^{-7} Ω^{-1} cm^{-1} at 200 °C. Extrapolating the present high temperature total conductivity to room temperature yields $\sigma_{tot} \approx 10^{-13}$ Ω^{-1} cm^{-1} for KO_2.

Before discussing the pO_2 dependence, it is indispensable to check the thermodynamic stability window which to the low pO_2 side is determined by the coexistence with the respective peroxide. According to the thermochemical data published in ref.[33], CsO_2 and KO_2 decompose into the peroxides below 10^{-6} bar pO_2 and 10^{-3} bar at 250 °C. No data are known for RbO_2, but the decomposition-pO_2 of RbO_2 can be expected to lie in between the values for CsO_2 and KO_2. The stability of KO_2, RbO_2, and CsO_2 was verified by annealing the powders at defined pO_2 and T for 48 h, quenching them to room temperature and checking for peroxide peaks in Raman spectra.[41] At 250 °C both CsO_2 and RbO_2 are stable at $pO_2 = 10^{-5}$ bar, while KO_2 decomposes to the peroxide already at 10^{-3} bar O_2. To extend the accessible pO_2 range for KO_2, the maximum measurement temperature for KO_2 was restricted to 225 °C, where it is found to be stable down to $pO_2 = 10^{-4}$ bar.

The pO_2 dependence of the conductivities of KO_2, RbO_2, and CsO_2 is depicted in **Figure 3**. At low pO_2, the total bulk conductivities of KO_2, RbO_2, and CsO_2 decrease with increasing pO_2 (with a slope of ≈–0.5) and move into a plateau for higher pO_2. For as-prepared KO_2, the plateau extends almost over the entire studied pO_2 range and the conductivity begins to significantly increase only at 10^{-4} bar pO_2. The data were obtained by measuring from high to low pO_2 with about 24 h equilibration time at each pO_2. For as prepared KO_2, RbO_2, and CsO_2, the conductivities are fairly reproducible upon repeating the measurement (with a deviation of about 10% for CsO_2 and RbO_2 and 20% for as prepared KO_2). For annealed KO_2, the conductivity in the plateau increased by a factor of two within 2 weeks measurement. The absence of pronounced ageing phenomena suggests that dislocations—since expected to form in the plastic deformation during pellet pressing at 25 °C and to (partially) anneal out during the elevated measurement temperature—do not strongly affect the measured conductivities.[42]

In the range of pronounced pO_2 dependence of the conductivity for CsO_2 and RbO_2, conductivity relaxation after a sudden pO_2 change (cf. Figure S5, Supporting Information) can be used to investigate equilibration kinetics with the gas phase. The relaxation time shows no significant pO_2 dependence (in the range 1 to 10^{-5} bar), opposite to what is expected for surface controlled kinetics (which is generally expected to exhibit a strong increase of reaction rate with increasing pO_2, typically a power law with exponent larger than 0.5[43]). Hence, the oxygen equilibration of the sample can be considered to be diffusion controlled. The chemical diffusivity D^{δ} obtained from the exponential resistance decay[44] at long times is shown in **Figure 4** (for RbO_2 no D^{δ} measurements were possible below 225 °C because then the conductivity became pO_2-independent).

Having presented their total conductivities, let us now analyze the defect chemistry of the superoxides in greater detail. As-prepared KO_2 behaves differently from the other samples, exhibiting a pronounced pO_2 independent regime (Figure 3b). This suggests that this sample contains additional point defects acting as pO_2 independent dopants, the concentration of which strongly decreases by the annealing procedure. In principle

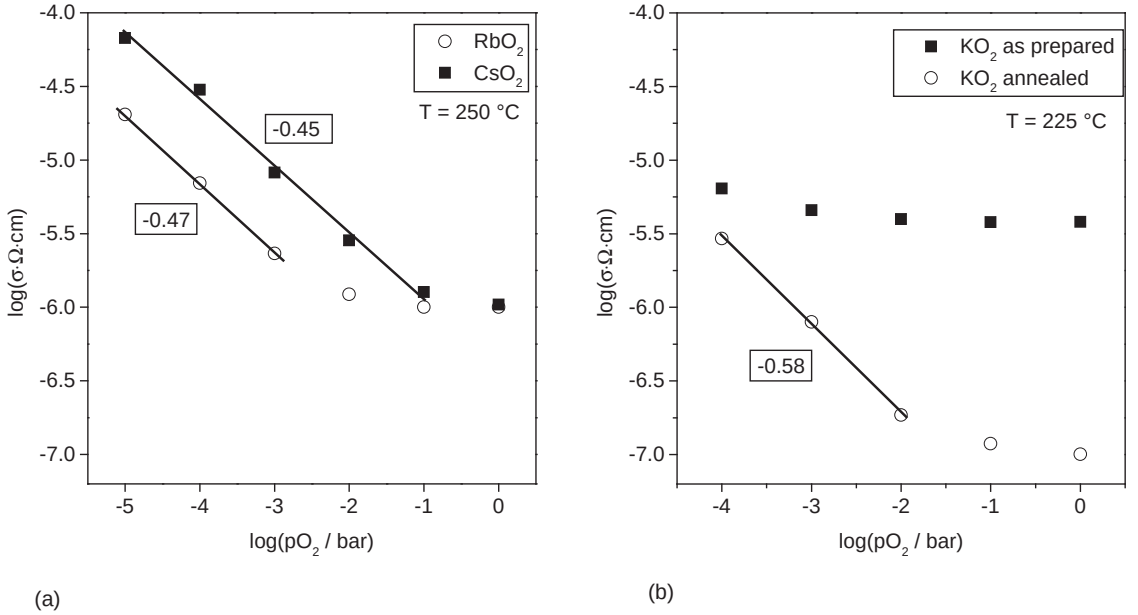

Figure 3. Oxygen partial pressure dependence of the total bulk conductivity from electrochemical impedance spectroscopy of a) CsO_2 (solid squares) and RbO_2 (open circles) at 250 °C and b) as prepared (solid squares) and annealed KO_2 (open circles) at 225 °C.

© 2015 WILEY-VCH Verlag GmbH & Co. KGaA, Weinheim

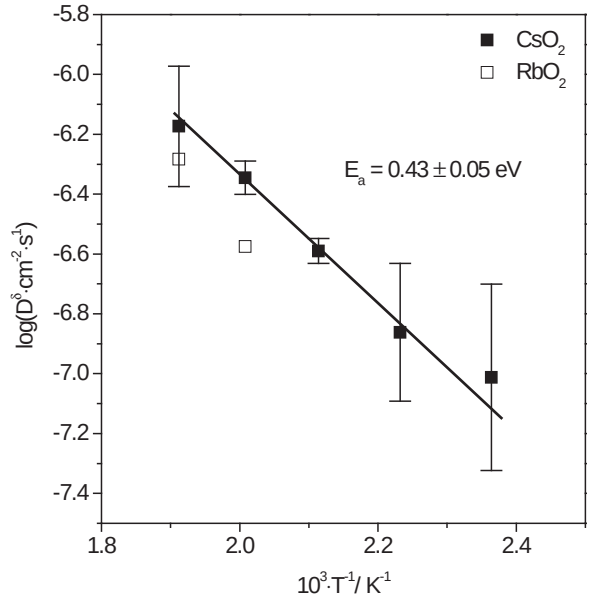

Figure 4. Temperature dependence of the chemical diffusivity D^{δ} of CsO_2 (solid squares) and RbO_2 (open squares) from conductivity relaxation measurements from 10 to 100 ppm pO_2. No reliable data were obtained for RbO_2 < 225 °C because the pO_2 dependence of the bulk resistance is only weak at these temperatures.

aliovalent metal cation impurities could precipitate into a secondary phase upon annealing; yet, no metal impurities with valence >1 (donors) have been detected by inductively coupled plasma optical emission spectroscopy (ICP–OES). One could imagine that native defects remain from synthesis conditions and have much longer equilibration times than the other defects (superoxide vacancies or alkali interstitials, see below), i.e., they are effectively frozen at 250 °C and equilibrated away in the annealing step. Such frozen-in species could be oxide ions on superoxide sites O'_{O_2} (which were identified, e.g., in barium peroxide single crystals by X-ray diffraction[45]), peroxide ions O'_{2O_2} (although for peroxides it is difficult to imagine that they are frozen at 250 °C while superoxide ions equilibrate with the gas phase) or potassium vacancies. The presence of O'_{O_2} or O'_{2O_2} corresponds to conditions of lower effective pO_2, which may (locally) prevail during the synthesis of KO_2 from potassium metal. Hypothetically, the as-prepared KO_2 might contain a high number of charged extended defects, such as dislocations formed during cold-pressing, which cause an appreciable conductivity and which are healed out during the annealing step. It is, however, not obvious why dislocation effects should be more pronounced in KO_2 than in RbO_2, CsO_2.

Now let us concentrate on the stationary behavior. The negative slope of the pO_2 dependence of the total conductivity of CsO_2, RbO_2 and annealed KO_2 at low pO_2 indicates excess electron conduction, or ion conduction via positively charged defects such as metal interstitials or superoxide vacancies (more discussion on this below in the derivation of the defect model). For the actual identification of the main charge carriers the separation of the electronic and ionic partial conductivities is required, which is often performed with DC stoichiometry polarization measurements. For ionically blocking dense gold electrodes, the steady-state current at sufficiently long polarization times is carried only by electronic carriers (as long as "leakage currents" by oxygen exchange reaction with the gas phase are negligible). The cells Au | MO_2 | Au (M = K, Rb, Cs) yield an apparent electronic conductivity of CsO_2, RbO_2 and annealed KO_2 that is comparable to the ionic conductivity at 1 bar pO_2 (Figure S6, Supporting Information).

For a mixed conductor with sufficiently high ionic transference number (t_{ion}), t_{ion} values can also be determined by EMF measurements. Here, the two sides of a sample pellet are exposed to different oxygen activities and the EMF across the sample is measured with an electrometer of high input resistance. For not too large pO_2 differences (and for a measurement time that is much shorter than the oxygen equilibration time with the bulk of the sample, so that the bulk defect concentrations can be assumed to remain constant), the ionic transference number t_{ion} can be obtained from the ratio of the measured EMF and the Nernst voltage which assumes an electrolyte with an ionic transference number of unity (here with $z = 1$, since only one electron is exchanged per O_2 molecule in the electrode reaction for alkali metal superoxides):

$$t_{ion} = \frac{\mathrm{EMF}}{\frac{RT}{F}\ln\frac{pO_2(2)}{pO_2(1)}} \quad (1)$$

The ionic transference number and the total bulk conductivity σ_{bulk} from impedance spectroscopy yield the partial ionic and electronic conductivities according to $\sigma_{ion} = t_{ion} \times \sigma_{bulk}$ and $\sigma_{eon} = (1 - t_{ion}) \times \sigma_{bulk}$.

The EMF response of the cell $pO_2(1)$ | Pt | CsO_2 | Pt | $pO_2(2)$ with $pO_2(1)$ = 1 bar and $pO_2(2)$ = 1 or 0.1 bar at 175 °C is shown in **Figure 5**. The relaxation time of the voltage response shown in the inset is about 8 s in the temperature range 175–250 °C, which corresponds to the flush time of the reactor. Below 175 °C, the EMF response time significantly increases suggesting that then the oxygen reduction/superoxide oxidation becomes

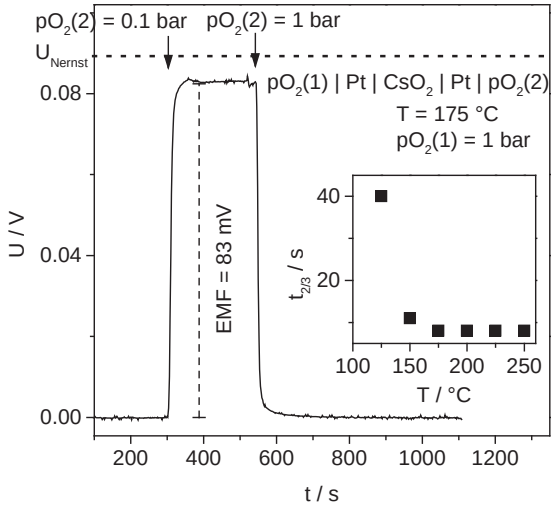

Figure 5. EMF response of the cell $pO_2(1)$ | Pt | CsO_2 | Pt | $pO_2(2)$ with $pO_2(1)$ = 1 bar and $pO_2(2)$ = 1 or 0.1 bar at 175 °C. The inset shows the time to reach 2/3 of the final voltage response versus temperature.

© 2015 WILEY-VCH Verlag GmbH & Co. KGaA, Weinheim

limiting. The measured EMF values of the cells $pO_2(1)$ | Pt | MO_2 | Pt | $pO_2(2)$ (with M = K, Rb, and Cs) correspond to 90%–100% of the Nernst voltage for $pO_2(1) = 1$ bar and $pO_2(2) = 0.1$ bar as well as for $pO_2(1) = 10^{-3}$ bar and $pO_2(2) = 10^{-4}$ bar, i.e., the EMF losses due to electronic conduction are ≤10% at both high and low pO_2.

Bearing in mind that the DC measurements indicated a fairly balanced mixed conductivity, these values are comparably high (but nevertheless *both* approaches agree in finding that the conductivity is *not* predominantly electronic). It is thus obvious that the apparent electronic conductivity determined from DC polarization with gold electrodes overestimates the true electronic conductivity of the alkali superoxides, suggesting that the sputtered gold electrodes do not sufficiently block the ionic carriers but allow perceptible oxygen exchange reaction and thus leakage current (in particular at high pO_2 where typically gas exchange rates are higher). The EMF losses of few mV are too small and too close to the experimental errors (such as the uncertainty with regards to the exact pO_2 at the electrodes) to extract reliable values of electronic conductivity (or its pO_2 dependence). Thus, only an upper limit of $\sigma_{eon} \leq 0.1 \times \sigma_{ion}$ can be provided for CsO_2, RbO_2, and as-prepared/annealed KO_2. Hence, the electrical conductivities of CsO_2, RbO_2, and KO_2 are predominantly determined by ionic transport in the measured temperature and oxygen partial pressure ranges, similar to the findings for Li_2O_2.[24]

Let us now develop a defect chemical model based on the experimental results. For brevity, the defects are denoted in the Kröger–Vink notation[46] which indicates the type of structure element by the main letter (*V* for a vacancy, *M* and *O* for alkali and oxygen ions), the site of the defect by the subscript (*i* for an interstitial site, *M* and O_2 for the regular lattice sites of alkali and superoxide ions), and the charge relative to the perfect lattice by the superscript (dot and dash for a single positive and negative relative charge, double-dot and double-dash for double charges). The possible ionic defects in these superoxides are metal ion vacancies ($V_M^{'}$), metal ion interstitials ($M_i^{\bullet}$), superoxide vacancies ($V_{O_2}^{\bullet}$) and superoxide interstitials ($O_{2_i}^{'}$). Furthermore, it is conceivable that the superoxide site might be occupied by an oxide ion O^{2-} yielding an oxide defect ($O_{O_2}^{'}$) with a negative charge relative to the perfect lattice. As derived from the following reactions, the positive defects are expected to exhibit increasing concentrations at lower pO_2. Decreasing pO_2 increases the superoxide vacancy concentration:

$$O_{2_{O_2}}^{x} \rightleftharpoons V_{O_2}^{\bullet} + O_2(g) + e' \quad (2)$$

Via Schottky and Frenkel reaction this increased $[V_{O_2}^{\bullet}]$ also enhances the concentration of alkali interstitials:

$$M_M^x + O_{2_{O_2}}^x \rightleftharpoons V_M^{'} + V_{O_2}^{\bullet} + MO_2 \quad (3)$$

$$M_M^x + V_i^x \rightleftharpoons V_M^{'} + M_i^{\bullet} \quad (4)$$

On the other hand, the concentrations of alkali metal vacancies and superoxide interstitials increase with increasing pO_2, thus they cannot be responsible for the conductivity increase with decreasing pO_2. Thus, the majority ionic charge carriers in CsO_2, RbO_2, and annealed KO_2 are alkali metal interstitials and/or superoxide vacancies. The oxide defect $O_{O_2}^{'}$ represents a special case: although negatively charged, its concentration increases with decreasing pO_2 because its formation requires conduction electrons (see Equation (6) in **Table 1**). However, as shown below, this defect would lead to a more negative pO_2 dependence of the ionic conductivity than the measured −1/2 (Figure 3).

Table 1. Main defect chemical reactions and corresponding mass action laws for alkali superoxides.

	Reaction		Mass action law
Band–band reaction	$0 \rightleftharpoons e' + h^{\bullet}$		$K_B = n \cdot p$
Schottky reaction	$M_M^x + O_{2_{O_2}}^x \rightleftharpoons V_M^{'} + V_{O_2}^{\bullet} + MO_2$	(3)	$K_S = [V_M^{'}] \cdot [V_{O_2}^{\bullet}]$
Frenkel reaction	$M_M^x + V_i^x \rightleftharpoons V_M^{'} + M_i^{\bullet}$	(4)	$K_F = [V_M^{'}] \cdot [M_i^{\bullet}]$
Superoxide dissociation (into oxide defects)	$O_{2_{O_2}}^x + V_{O_2}^{\bullet} + 3e' \rightleftharpoons 2O_{O_2}^{'}$	(6)	$K_O = \frac{[O_{O_2}^{'}]^2}{[V_{O_2}^{\bullet}] \cdot n^3}$
Gas phase exchange	$O_{2_{O_2}}^x \rightleftharpoons V_{O_2}^{\bullet} + O_2(g) + e'$	(2)	$K_G = [V_{O_2}^{\bullet}] \cdot n \cdot pO_2$

To further distinguish between alkali metal interstitials and oxygen species, electrochemical cells employing alkali tungsten bronzes as electrodes reversible for exchange of alkali ions and electrons were investigated. These electrode materials combine high electronic and alkali metal ion conductivity with chemical stability and are expected not to exchange superoxide ions reversibly with the sample. According to the impedance spectra of the cells $K_{0.3}WO_3$ | KO_2 | $K_{0.3}WO_3$ and $Cs_{0.3}WO_3$ | CsO_2 | $Cs_{0.3}WO_3$ shown in **Figure 6** (clearly exhibiting the beginning of an electrode arc extending to very low frequencies), the electrodes are blocking for the dominating ionic charge carrier,[47] which supports that superoxide vacancies contribute considerably to the ionic transport in these materials (but a minor contribution from alkali interstitials is still possible). The ^{18}O exchange experiments reported at the end of this publication further support the presence of mobile $V_{O_2}^{\bullet}$. It is noteworthy that recently a $RbO_{1.72}$ phase was reported to have a structure that can be regarded as RbO_2 containing a high concentration of anion vacancies (no superstructure peaks related to ordering of the vacancies were observed).[48]

The basic defect reactions as well as the mass action laws for a quantitative analysis of the pO_2 dependences are summarized in Table 1. In the electroneutrality condition also acceptor A′ and donor $D^{\bullet}$ impurities have been included:

$$n + [V'_M] + [O'_{O_2}] + [A'] = p + [M_i^{\bullet}] + [V_{O_2}^{\bullet}] + [D^{\bullet}] \quad (5)$$

Analytical expressions for the dependencies of the defect concentrations on pO_2 or alkali metal activity can be obtained by reducing Equation (5) to a single term on each side (Brouwer approximation[49]), i.e., only the negatively and positively charged majority defects are taken into account for a limited range of pO_2/metal alkali activity. We will briefly discuss these

© 2015 WILEY-VCH Verlag GmbH & Co. KGaA, Weinheim

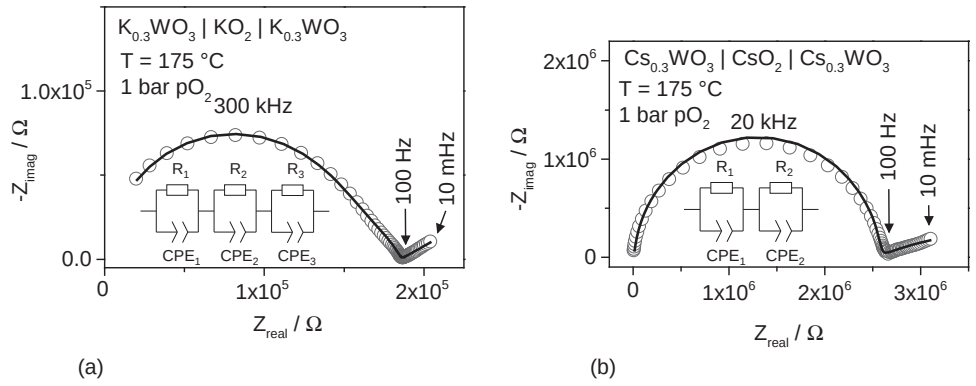

Figure 6. Impedance spectra of the cells a) $K_{0.3}WO_3$ | KO_2 (as prepared) | $K_{0.3}WO_3$ and b) $Cs_{0.3}WO_3$ | CsO_2 | $Cs_{0.3}WO_3$ at 175 °C and 1 bar pO_2. The bulk resistances R_1 are comparable to samples with gold electrodes. The additional relaxation process at mid frequencies (with a capacitance of 10^{-9} F) in the spectrum of $K_{0.3}WO_3$ | KO_2 (as-prepared) | $K_{0.3}WO_3$ is not observed in the spectra of as-prepared potassium superoxide with gold or platinum electrodes; it is therefore assigned to a reaction layer between $K_{0.3}WO_3$ and KO_2. Note that for CsO_2, this feature is absent, but still an electrode arc is observed.

regimes, and derive a Kröger–Vink diagram from these considerations (**Figure 7**).

For the situation in which superoxide vacancies are predominantly compensated by electrons, the electroneutrality condition is simplified to $n = [V_{O_2}^{\bullet}]$ and the mass action law of the gas phase reaction (2) yields the relation $[V_{O_2}^{\bullet}] = K_G^{1/2} \cdot pO_2^{-1/2}$. The exponent of −1/2 corresponds very well to the experimentally observed slope of ≈0.47–0.58 in the plot of logσ versus logpO_2 (for CsO_2, RbO_2, and annealed KO_2 at low pO_2, Figure 3). Note that the same pO_2 dependence (with $K_S^{-1}K_F \cdot K_G^{1/2}$ as proportionality factor) is obtained for alkali metal interstitials via the Schottky and Frenkel reactions, but the presence of an electrode arc in Figure 6 indicates they are not the main ionic carrier. The decreasing slope at high pO_2 could be explained by the transition into a regime controlled by the pO_2 independent Schottky reaction (3). The dependence of the defect concentrations on pO_2 (and correspondingly on metal activity) for this case is shown in Figure 7a. While this defect model can account for the pO_2 dependence at elevated temperatures, it fails to explain the decreasing activation energy with increasing pO_2 as shown in Figure 2 and **Table 2** (note that the conductivity is predominantly ionic at low as well as at high pO_2, i.e., the same defect

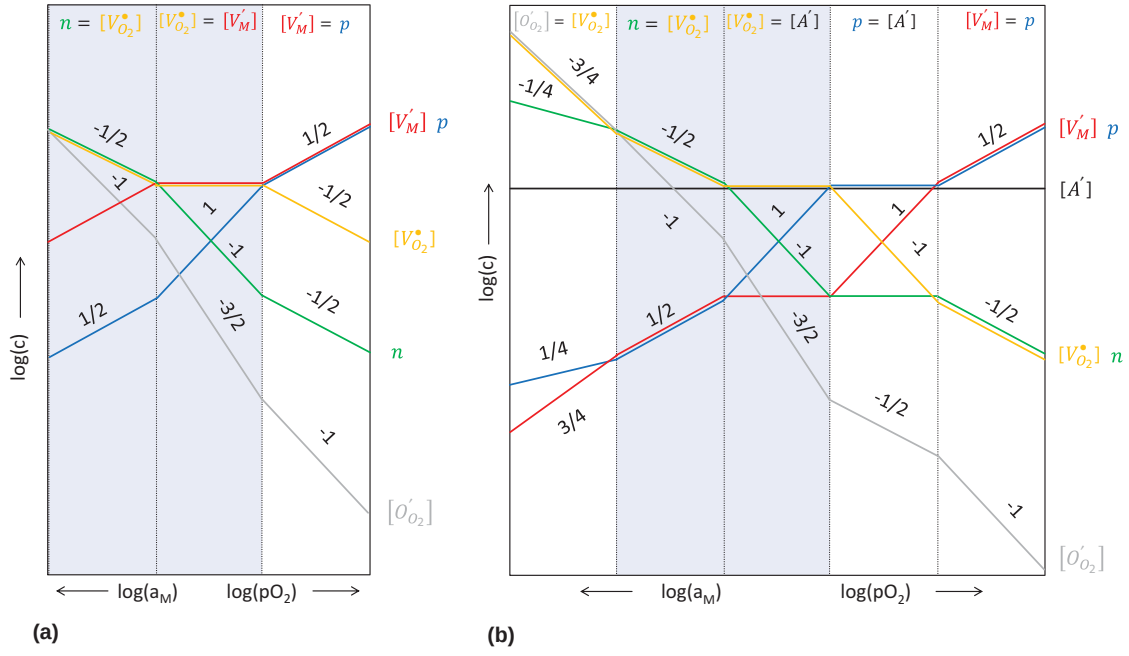

Figure 7. Dependence of defect concentrations on pO_2 and metal activity for alkali superoxides (Kröger–Vink diagram). The simplest case with only intrinsic defects is shown in a), while oxide defects O'_{O_2} and acceptors A′ are included as charge compensating species in (b). The relevant regimes in accordance with the experimentally observed pO_2 dependence of RbO_2, CsO_2, and annealed KO_2 are indicated in light blue. If the oxide defect O'_{O_2} has a low mobility and is effectively frozen-in at measuring temperature, it can take the function of the pO_2-independent acceptor A′. Note that the cases $n = [V_{O_2}^{\bullet}]$ and the hypothetical alternative $n = [M_i^{\bullet}]$ lead to identical slopes and are thus not drawn separately. The defect model assumes that Frenkel and Schottky reactions (3) and (4) are in equilibrium.

© 2015 WILEY-VCH Verlag GmbH & Co. KGaA, Weinheim

Table 2. Summary of conductivity activation energies from Figure 2, given in eV.

Regime		As-prepared KO_2	Annealed KO_2	RbO_2	CsO_2
High pO_2	Whole T range	0.72 ± 0.02	0.43 ± 0.01	0.76 ± 0.05	0.47 ± 0. 04
Low pO_2	High T	0.75 ± 0.02	1.3 ± 0.03	1.1 ± 0.04	0.98 ± 0.02
	Low T		0.43 ± 0.01		0.50 ± 0.02

migration energy applies). This decrease is most likely due to a regime at high pO_2 in which the concentration of the compensating negative defect is constant (e.g., a frozen-in native defect such as O'_{O_2}, or other impurity), i.e., the activation energy consists only of the ionic defect migration energy. Such a situation is depicted in Figure 7b.

Within this defect model, an increase of electron concentration with decreasing pO_2 is expected. The EMF measurements did not allow drawing a direct reliable conclusion about the pO_2 dependence of σ_{eon}. Nevertheless, given that all superoxides studied here have a band gap exceeding 2 eV as judged from the yellow color of the superoxides, the electroneutrality condition $n = [V^{\bullet}_{O_2}]$ relevant for the low pO_2 regime implies that $n >> p$.[50] Thus, for roughly comparable mobility of n- and p-type carriers the electronic conductivity can be safely assigned to be n-type. The estimated low hole concentration is related to holes (expected to be localized, cf. hole localization in Li_2O_2 as described below) being enegetically unfavorable species in the alkali superoxides: they correspond to either an alkali metal ion with a very unusual valence of +2 or a neutral oxygen molecule in an ionic lattice.

The Kröger–Vink diagram has been extended by a regime controlled by equilibrated oxide defects O'_{O_2} at extremely low pO_2 leading to an exponent of σ_{ion} of −3/4, which however is experimentally not observed in the investigated partial pressure range $pO_2 \geq 10^{-5}$ bar. It should be pointed out that not all regimes are necessarily experimentally accessible and relevant. The O'_{O_2} controlled regime at very low oxygen partial pressure might be outside the stability limit of the alkali superoxides at temperatures that enable thermodynamic equilibrium with the gas phase. Lacking quantitative data on the defect concentrations, the onset of the regime with p-type electronic conductivity on the right hand side can be estimated only very roughly,[51] and probably lies outside the relevant condition window for an alkali–metal battery (even if it operates under pressurized O_2, or develops local oxygen overpressure).

Analogous to the situation in Li_2O_2 where holes as dominating electronic defect were found to be localized on the molecular oxygen species (experimentally,[24] as well as in ab initio calculations, e.g., refs.[21–23]), it is expected that excess electrons in alkali superoxides are also localized forming peroxide ions on superoxide sites (cf. the small width of the valence band in density functional theory calculations for NaO_2, KO_2, and RbO_2[52–54]). Since at low pO_2 according to the electroneutrality condition $n = [V^{\bullet}_{O_2}]$ but the conductivity remains predominantly ionic, this implies that for the alkali superoxides in the investigated temperature range the mobility of the ionic carriers exceeds that of the electrons. Corresponding to their localized nature, the excess electrons as small polarons will exhibit a perceptible migration barrier. It is important to note that the lowest activation energies found for the total ≈ ionic conductivity (Table 2) of 0.43–0.5 eV are not so far from typical polaron migration barriers in related systems (e.g., ≥0.4 eV for Li_2O_2 from ab initio calculations[22,23]). The long distance of 3.43–4.02 Å between O atoms of neighboring superoxide ions and the fact that the superoxide ions are not arranged in straight lines (Figure S3, Supporting Information) is also expected to decrease the electron mobility.

In general, the conductivity activation energy comprises contributions from defect migration and formation enthalpies. However, in the high pO_2 regime the measured conductivity is pO_2 independent for all samples, indicating that the concentration of mobile ionic defects is fixed (extrinsic regime). Then the observed activation energy directly corresponds to the migration enthalpy. According to the first row in Table 2, the migration enthalpies for ionic conductivity (predominantly by superoxide vacancies) range from 0.43 to 0.70 eV. It is remarkable that this value is lower than the typical 0.8 eV observed for oxygen vacancies V_O in most perovskites.[55,56] Another interesting observation is that the activation energy for as-prepared KO_2 is significantly higher than for annealed KO_2 although both samples are predominantly ionic conductors. This could be due to defect association with the high concentration of negative defects in as-prepared KO_2 (note that also for Li_2O_2 perceptible ionic defect association was found[24]). In the limit of strong association, the observed difference in activation energies of ≈0.3 eV would correspond to half the association enthalpy.

At low pO_2 (second row in Table 2) the behavior is more complex. As-prepared KO_2 exhibits the same activation energy as in high pO_2, consistent with its pO_2 independent conductivity. At low T and pO_2, annealed KO_2 has a similar E_a as in high pO_2, while at high T a larger activation energy is found. This behavior may originate from two effects: i) the extrinsic regime extends over a larger pO_2 range at lower T and/or ii) at sufficiently low T, the oxygen exchange reaction determining $[V^{\bullet}_{O_2}]$ in the intrinsic regime is kinetically frozen in. For both cases E_a in the intrinsic high-T regime comprises also defect formation contributions. A similar situation is found for CsO_2. Within the suggested defect model, the difference between the activation energies at low and high temperature corresponds to half of the standard reaction enthalpy of Reaction (2). Thus, ΔH_G^0 is about 1 eV for CsO_2 and 1.7 eV for annealed KO_2. The absence of a low E_a regime for RbO_2 at low pO_2 cannot be explained at the moment.

Within this defect model we can now also interpret the activation energies of D^{δ} in Figure 4. The chemical diffusion coefficient can be expressed by[57]

$$D^{\delta} = \frac{RT}{F^2}\frac{\sigma_{ion}\sigma_{eon}}{\sigma_{total}}\left(\frac{1}{[\text{ionic defect}]} + \frac{1}{n}\right) \quad (6)$$

In this expression the excess electron concentration n can equivalently be expressed by the peroxide concentration $[O'_{2_{O_2}}]$

© 2015 WILEY-VCH Verlag GmbH & Co. KGaA, Weinheim

(owing to very low orbital overlap between neighboring molecular oxygen anions, conduction electrons can be considered to be localized as peroxide ions on superoxide sites $O'_{2_{O_2}}$). In Equation (7), further trapping effects (defect association reactions) are ignored. The ionic defects can be superoxide vacancies and/or alkali interstitials, i.e., are always singly positively charged, and in the pO_2-dependent regime compensated by the excess electrons:

$$D^{\delta} = \frac{RT}{F^2}\sigma_{\text{ion}} t_{\text{eon}} \left(\frac{2}{[\text{ionic defect}]} \right) = 2D_{\text{ion}} t_{\text{eon}} \tag{7}$$

considering that $\sigma_{\text{total}} \approx \sigma_{\text{ion}}$. When t_{eon} has only a slight temperature dependence (as suggested for the superoxides investigated here from *T*-dependent EMF measurements), the activation energy of the chemical diffusion coefficient should largely be determined by E_a of the ionic defect diffusivity. Indeed the activation energy of for CsO_2 (0.45 eV at 150–250 °C, low pO_2, Figure 4) agrees within the error bars with the activation energy of the ionic conductivity (0.5 eV, Table 2) in the intrinsic regime. For RbO_2 unfortunately the temperature range in which the conductivity is pO_2-dependent (and thus D^{δ} can be determined at all) is too limited to extract a reliable activation energy of D^{δ}.

2.2. Gas Phase Analysis of ^{18}O Exchange

The fast EMF response of the studied alkali superoxides even at low temperature and the comparably high chemical diffusivity and conductivity of oxygen species suggest that oxygen exchange might be fast in these materials. The kinetics of the oxygen exchange was further studied by exchanging 16- by 18-oxygen isotopes (and vice versa) in powder samples of K, Rb, and Cs superoxide monitoring the gas phase composition by mass spectrometry. Insight into the mechanism of oxygen transport can be obtained from the formation or absence of mixed species $^{16}O^{18}O$ (its presence implies that O_2 was dissociated in the exchange process). The first important question is if only a surface layer of oxygen can be exchanged, or the whole sample volume (the fact that pO_2 changes lead to a stoichiometry relaxation a from which D^{δ} was extracted does not guarantee the stoichiometry change occurs by oxygen diffusion; to some degree (and depending on the alkali ion) it can also occur by alkali diffusion, and this transport cannot contribute to oxygen isotope exchange). To answer this point we decided to perform isotope exchange under steady flow conditions which allow us to determine the overall exchanged amount of oxygen from an integration (on the time scale) of the measured isotope concentrations. In particular, we first have to establish if the assumptions required for application of pulse isotope exchange (fast transport from surface into bulk)[58] are fulfilled. A more detailed mechanistic investigation of the oxygen exchange surface reaction is beyond the scope of the present study and will be published separately.

Figure 8 shows the evolution of the ion currents (proportional to the concentrations, ideally with same sensitivity factor for m = 32, 34, and 36) of $^{16}O_2$, $^{16}O^{18}O$, and $^{18}O_2$ when the superoxide powder (previously equilibrated with $^{18}O_2$) is exposed to a flow of 3 mL min^{-1} $^{16}O_2$ with the respective oxygen partial pressure. For all investigated superoxides, the integration of ^{18}O flux in the exhaust gas indicates that essentially all oxygen contained in the sample was exchanged (not only a surface monolayer). This means that at 200 °C—independent of mobile cation defects—also oxygen is mobile in these materials over a micrometer length scale within a few hours. In order to decide if this oxygen exchange is limited by the surface reaction or bulk transport within the grains, the experiments were performed in different pO_2. The measurements for KO_2 in various pO_2 show two important features: i) the amount of $^{34}O_2$ decreases strongly with increasing pO_2 and ii) the characteristic decay times decrease strongly with increasing pO_2 (for $^{36}O_2$ more strongly than for $^{34}O_2$). Since bulk oxygen transport is expected to decelerate with increasing pO_2 (as it requires defects with negative pO_2 dependence such as $V^{\bullet}_{O_2}$ or O'_{O_2}), point (ii) indicates that the oxygen exchange is indeed limited by the surface reaction (which is typically accelerated by larger pO_2). The decay time of the $^{34}O_2$ and $^{36}O_2$ curves is inversely proportional to the effective surface rate constant k^*.[59] The larger pO_2 dependence of the decay time of the $^{36}O_2$ signal (largely arising from molecular oxygen exchange without O—O bond breaking) compared to $^{34}O_2$ (requiring dissociation) naturally explains the larger $^{34}O_2$ fraction found at low pO_2. While a detailed discussion of the two competing reaction pathways (dissociative vs molecular exchange) requires further investigation, a larger pO_2 dependence of the effective exchange rate for the molecular exchange appears very plausible since this mechanism will definitively contain molecular oxygen species in its rate-determining step (i.e., has a reaction order of one for O_2).

When we compare the $^{34}O_2$ fraction for the different superoxides at the same pO_2 (K, Rb, and Cs in 1% O_2; K and Rb in 10% O_2), it is generally higher for KO_2 than for RbO_2 and CsO_2, i.e., in the heavier alkali superoxides the concentration (and/or mobility) of $V^{\bullet}_{O_2}$ into which adsorbed O_2^- can be incorporated without dissociating seems to be higher. This is in line with the expansion of the lattice constant upon introducing heavier alkali ions (leading also to larger free volume in the unit cell) as well as increased polarizability which are expected to facilitate the migration of molecular ions in the lattice. A further decrease of $V^{\bullet}_{O_2}$ mobility for NaO_2 with even smaller lattice constant might be anticipated, but lacking experimental data on NaO_2 such a statement remains speculative (at any rate, ^{18}O exchange on powder samples with the kinetics being surface reaction limited supplies only a lower limit for bulk oxygen diffusivity).

In order to quantitatively determine the effective rate constants k^*, the grain diameter must be known. For the present samples this is a challenge due to the extremely high reactivity of CsO_2 and KO_2 with CO_2 and H_2O (e.g., for scanning electron microscopy first an appropriate transfer box excluding air contact has to be developed). Thus presently we roughly estimate the grain size to be about 500 nm. Using this value, we obtain k^* values in the range of 3×10^{-9}–1×10^{-8} cm s^{-1} for K, Rb, and Cs superoxide at 200 °C and $pO_2 = 0.01$ bar. It is worthy of note that this estimate is more than nine orders of magnitude higher than the respective k^* value (extrapolated to 200 °C with its activation energy of 2.7 eV determined at 600–900 °C) for slightly Fe-doped $SrTiO_3$ (a perovskite with 3 eV band gap, requiring dissociation of the O—O bond upon incorporation).[60] It still exceeds the extrapolated k^* for Y-doped ZrO_2 (where below 700 °C the activation energy was found to drop to 0.7 eV)

© 2015 WILEY-VCH Verlag GmbH & Co. KGaA, Weinheim

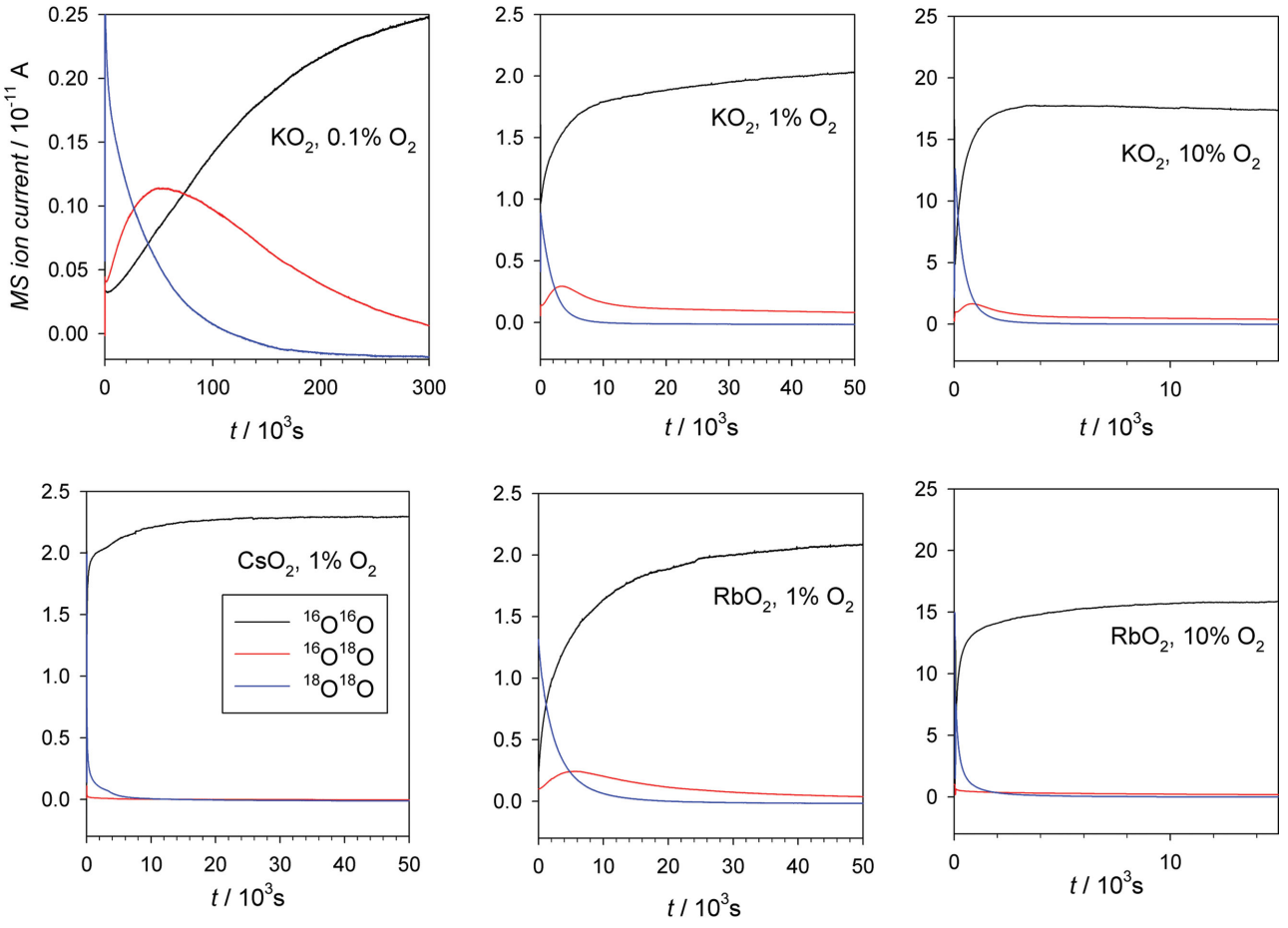

Figure 8. Mass spectrometry signals of $^{16}O^2$, $^{16}O^{18}O$, and $^{18}O_2$ for as-prepared KO_2 powder samples in a flow of 0.1% $^{16}O_2$, 1% $^{16}O_2$, and 10% $^{16}O_2$ (top row, note the different time scales) and CsO_2 (in 1% O_2) and RbO_2 (in 1% O_2 and 10% O_2) powder samples at 200 °C after switching from equilibration in the respective $^{18}O_2$ gas mixture to $^{16}O_2$ gas mixture.

by four orders of magnitude.[61] The k^* values of the superoxides are even larger by 1/2 to 1 order of magnitude than that of $SrFe_{0.35}Ti_{0.65}O_{3-\delta}$ and $SrFe_{0.5}Ti_{0.5}O_{3-\delta}$ perovskites (extrapolated to 200 °C) with high electronic conductivity.[62] Definitely, this fascinating fast surface kinetics merits more detailed investigation, keeping in mind that superoxide species may also be important intermediate species in catalytic reactions. It is well established that the cross-over from surface reaction to bulk diffusion limitation is given by k^*l/D^* (k^* = effective rate constant of tracer exchange, l = half sample thickness) being equal to D^*, with $k^*l < D^*$ indicating surface limitation.[63] Thus, from the estimated k^* values we can also derive a lower bound of D^* for oxygen species of about 7×10^{-14} cm^2 s^{-1} for K, Rb and Cs superoxide at 200 °C. According to the Nernst–Einstein equation, this corresponds to a lower bound of the contribution of oxygen defects to the ionic conductivity of 4×10^{-9} S cm^{-1}, which is in agreement with Figure 2.

3. Conclusion

The electrical transport properties of the superoxides of potassium, rubidium and cesium have been investigated by electrochemical methods. The total conductivity is in the range of 3×10^{-7}–5×10^{-6} S cm^{-1} at 200 °C for all three materials (and thus in the same range as for Li_2O_2). The main charge carriers in RbO_2 and CsO_2 have been shown to be superoxide vacancies in the investigated T and pO_2 range, while for KO_2 probably also K interstitials contribute significantly. The sign of the main electronic charge carrier (with $t_{eon} \leq 0.1$) could not be directly determined from experiments. However, according to the defect model verified by the experimental findings (e.g., increase of σ_{ion} with decreasing pO_2 in the intrinsic regime), the heavy alkali superoxides exhibit defect chemical regimes where the concentration of electrons largely exceeds those of the holes, and thus the alkali superoxides are most likely n-type semiconductors (with localized electrons in form of peroxide ions).

The gas-phase ^{18}O isotope exchange experiments evidence an almost complete oxygen exchange for KO_2, RbO_2, and CsO_2, i.e., perceptible concentration and mobility of defects in the oxygen sublattice. The fact that the amount of released $^{16}O^{18}O$ strongly decreases for high pO_2 and heavier alkali ions implies that superoxide ions are highly mobile in the lattice of KO_2, RbO_2, and CsO_2 as molecular units, without dissociation. The estimated lower limits for the effective rate constant of surface tracer exchange are many orders of magnitude

© 2015 WILEY-VCH Verlag GmbH & Co. KGaA, Weinheim

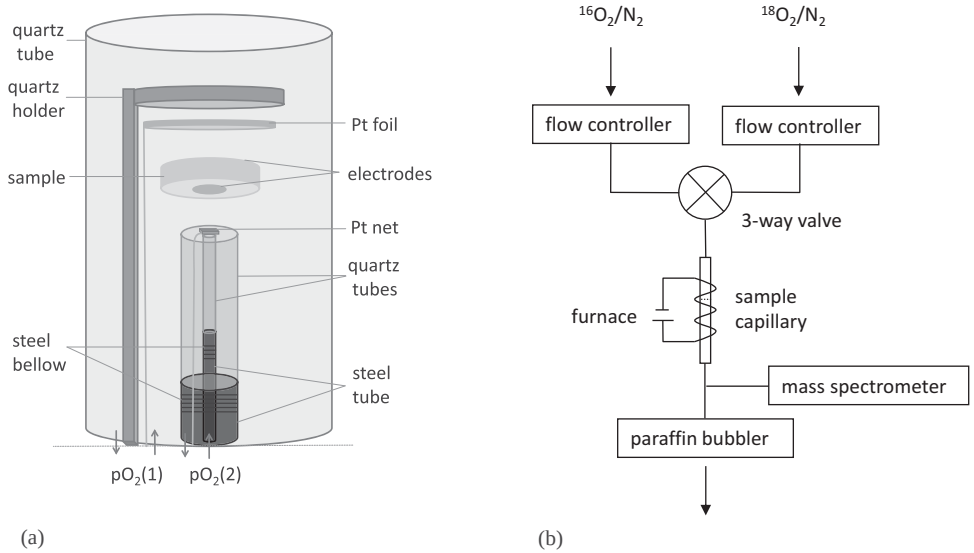

Figure 9. a) Schematic representation of the EMF and b) oxygen isotope exchange and gas phase analysis setup.

higher than for slightly Fe-doped $SrTiO_3$, a prototype mixed conductor.

Within the series of alkali–oxygen compounds, the strongest changes occur among the lighter members, e.g., the known tendencies in phase formation (peroxides for Li, peroxide and superoxide for Na, K depending on conditions, only superoxides for Rb, Cs). While Li and Na peroxides are p-type semiconductors (holes localized in form of superoxide ions on peroxide sites), the situation in inverted for KO_2, RbO_2, and CsO_2: n-type electronic conductivity (excess electrons localized in form of peroxide ions on superoxide sites). Regarding ionic carriers, defects in the cation lattice (lithium vacancies) dominate for Li_2O_2, whereas for the heavy alkali superoxides (KO_2 and particularly RbO_2 and CsO_2) superoxide vacancies prevail. Having extracted these trends from electrochemical experiments, ab initio calculations on defect formation and migration energies in these superoxides would now be highly welcome to obtain atomistic insight into their transport properties.

4. Experimental Section

All materials under investigation are extremely sensitive to humidity and CO_2, requiring handling in a glove box or gastight sample holders under inert gas or dry O_2 atmosphere. The alkali metals (distilled potassium, 99.95% metal purity, Sigma Aldrich; distilled cesium, 99.98% metal purity, Alfa Aesar, distilled rubidium, 99.75% metal purity, Alfa Aesar) were oxidized to the superoxides in home-made tantalum crucibles (from tantalum tubes of 99.95% metal purity, WHS Sondermetalle). Potassium superoxide was obtained by heating potassium metal to 250 °C (heating rate 200 °C h^{-1}) in 0.05 bar O_2 and subsequent annealing for 1 h in 1 bar O_2 at 250 °C. Rubidium and cesium superoxides were obtained by oxidation of the alkali metals to their suboxides[64] at room temperature by carefully adding O_2 via a needle valve (violent reaction!) and subsequent annealing for 1 h in 1 bar O_2 at 300 °C. KO_2 and RbO_2 powders are yellow, CsO_2 is dark yellow. Superoxide formation was confirmed by x-ray diffraction (XRD) and Raman spectroscopy (see Supporting Infromation). According to chemical analysis by ICP–OES, the main cation impurities are Na (700 ppm) and Li (10 ppm) in KO_2, Na (600 ppm), K (100 ppm), and Li (15 ppm) in RbO_2 and Na (700 ppm), K (20 ppm) and Li (5 ppm) in CsO_2. The main source of the Na impurity are the starting alkali metals (99.95% metals purity corresponds to 500 ppm impurities). These are isovalent impurities, i.e., they are not expected to act as dopants.[65] Alkaline earth metals (potential donor dopants) are below the detection limit of ICP–OES (i.e., $c_{Mg} + c_{Ca} + c_{Sr} + c_{Ba} < 20$ ppm). We do not have evidence for foreign elements acting as acceptors (this would require zero-valent elements on the alkali cation site or doubly charged anions on the superoxide site).Superoxide powders were uniaxially pressed with 250 MPa under argon into pellets with 5 mm diameter and ≈1 mm thickness. Owing to the high plastic deformability of the alkali superoxides ≥95% of the theoretical XRD density were obtained, but the pellets are dimensionally stable under measurement conditions (the qualitatively observed increase of plasticity from KO_2 to CsO_2 is parallel to a corresponding increase in compressibility[66]). One set of KO_2 pellets was annealed for 10 h at 450 °C in 1 bar pO_2 on MgO single crystals as support.

Platinum and gold electrodes (≈500 nm) were deposited by DC magnetron sputtering in a glove box. Alkali tungsten bronze powders for use as electrodes (M_xWO_3 with $x = 0.3$) were prepared by solid state reaction according to ref.[67] and pressed together with a sample powder layer with 250 MPa. Impedance spectra were recorded with a Novocontrol Alpha-A High Frequency Analyzer in the frequency range 10^6–10^{-2} Hz with 100 mV AC amplitude and fitted with the software ZView (Scribner Associates, Inc.). Oxygen partial pressures pO_2 were adjusted by mixing pure O_2 (5.0 purity), 1000 ppm O_2 in N_2 (5.0), and pure N_2 (5.0), and monitored by home-built lambda probes.

The setup for EMF measurements is schematically shown in **Figure 9**a. Steel bellows press the inner quartz tubes on the sample pellet. The innermost tube contacts the platinum net to the sample electrode; the larger tube separates the gas spaces (1) and (2). The contact between sample and quartz tube becomes sufficiently gastight (with flow rates of 80 and 100 mL min^{-1} for $pO_2(1)$ and $pO_2(2)$, where typically $pO_2(1) = 10 \times pO_2(2)$) without sealing agent by the plasticity of the sample at elevated temperature. The voltage was recorded with a Keithley electrometer 617. Freshly prepared $pO_2(1)$ | Pt | MO_2 | Pt | $pO_2(2)$ cells (with M = K, Rb, Cs) show large deviations from the expected zero baseline for $pO_2(1) = pO_2(2)$ and a sluggish voltage response upon switching to $pO_2(1) \neq pO_2(2)$. The freshly prepared sputtered Pt electrodes are relatively dense with a porosity below the resolution limit of scanning electron microscopy. The consequential insufficient amount of triple phase boundary impedes establishing the

© 2015 WILEY-VCH Verlag GmbH & Co. KGaA, Weinheim

equilibrium electrochemical potential of the electrons by the oxygen exchange surface reaction. The performance of the cells is greatly improved by a heat treatment at ≥225 °C, obviously leading to increased electrode porosity by Pt agglomeration (or some reaction of the alkali metal superoxides with the electrodes, e.g., to ternary oxides[68]).

The setup for oxygen isotope exchange and gas phase analysis is schematically represented in Figure 9b. The weighted sample (typically ≈20 mg) was filled in an argon glove box into a quartz capillary with a 10 mm thick bulge with glass frit (with 16–40 µm pores) supporting the powder. The capillary is sealed with 1/8 inch Swagelok ultratorr fittings and heated by a temperature controlled tube furnace. The gas inlet is connected to a three-way valve which enables switching between $^{16}O_2/N_2$ (commercial, 99.999% purity) and $^{18}O_2/N_2$ (home mixed, from $^{18}O_2$ with 97.1% isotopic purity from Euriso-Top and N_2 of 99.999% purity) gas mixtures (flow rate 3 mL min^{-1}). In some experiments the incorporation of ^{18}O into the sample was not performed under flowing gas but statically over an extended time with repeated flushing of the reactor to ensure complete exchange. After passing the sample capillary the gas is introduced via a leak valve into a Balzers Prisma quadrupole mass spectrometer to detect the oxygen isotope evolution (atomic masses 32, 34, and 36 corresponding to $^{16}O^{16}O$, $^{16}O^{18}O$, and $^{18}O^{18}O$). Excess gas is exhausted through a paraffin filled bubbler. The empty capillary was found to have a negligible oxygen exchange activity.

Supporting Information

Supporting Information is available from the Wiley Online Library or from the author.

Acknowledgements

The authors acknowledge F. Kögel for XRD, A. Schulz for Raman spectroscopy (Max Planck Institute for Solid State Research, Stuttgart, Germany), and A. Mayer for ICP–OES (Max Planck Institute for Intelligent Systems, Stuttgart, Germany).

Received: November 26, 2014
Revised: February 19, 2015
Published online: March 16, 2015

[1] K. M. Abraham, Z. Jiang, *J. Electrochem. Soc.* **1996**, *143*, 1.
[2] G. Girishkumar, B. McCloskey, A. C. Luntz, S. Swanson, W. Wilcke, *J. Phys. Chem. Lett.* **2010**, *1*, 2193.
[3] Y. C. Lu, D. G. Kwabi, K. P. C. Yao, J. R. Harding, J. Zhou, L. Zuin, Y. Shao-Horn, *Energy Environ. Sci.* **2011**, *4*, 2999.
[4] Z. Peng, S. A. Freunberger, Y. Chen, P. G. Bruce, *Science* **2012**, *337*, 563.
[5] D. G. Kwabi, N. Ortiz-Vitoriano, S. A. Freunberger, Y. Chen, N. Imanishi, P. G. Bruce, Y. Shao-Horn, *Mater. Res. Bull.* **2014**, *39*, 443.
[6] C. Xia, M. Waletzko, L. Chen, K. Peppler, P. J. Klar, J. Janek, *ACS Appl. Mater. Interfaces* **2014**, *6*, 12083.
[7] S. Nicola, *Nanotechnology* **2009**, *20*, 445703.
[8] M. K. Y. Chan, E. L. Shirley, N. K. Karan, M. Balasubramanian, Y. Ren, J. P. Greeley, T. T. Fister, *J. Phys. Chem. Lett.* **2011**, *2*, 2483.
[9] K. C. Lau, L. A. Curtiss, J. Greeley, *J. Phys. Chem. C* **2011**, *115*, 23625.
[10] M. Radin, F. Tian, D. Siegel, *J. Mater. Sci.* **2012**, *47*, 7564.
[11] M. D. Radin, J. F. Rodriguez, F. Tian, D. J. Siegel, *J. Am. Chem. Soc.* **2012**, *134*, 1093.
[12] K. C. Lau, R. S. Assary, P. Redfern, J. Greeley, L. A. Curtiss, *J. Phys. Chem. C* **2012**, *116*, 23890.
[13] V. Timoshevskii, Z. Feng, K. H. Bevan, J. Goodenough, K. Zaghib, *Appl. Phys. Lett.* **2013**, *103*, 073901.
[14] J. S. Hummelshøj, J. Blomqvist, S. Datta, T. Vegge, J. Rossmeisl, K. S. Thygesen, A. C. Luntz, K. W. Jacobsen, J. K. Nørskov, *J. Chem. Phys.* **2010**, *132*, 071101.
[15] Y. Mo, S. P. Ong, G. Ceder, *Phys. Rev. B* **2011**, *84*, 205446.
[16] J. Chen, J. S. Hummelshøj, K. S. Thygesen, J. S. G. Myrdal, J. K. Nørskov, T. Vegge, *Catal. Today* **2011**, *165*, 2.
[17] V. Viswanathan, K. S. Thygesen, J. S. Hummelshøj, J. K. Nørskov, G. Girishkumar, B. D. McCloskey, A. C. Luntz, *J. Chem. Phys.* **2011**, *135*, 214704.
[18] S. P. Ong, Y. Mo, G. Ceder, *Phys. Rev. B* **2012**, *85*, 081105.
[19] J. Kang, Y. S. Jung, S.-H. Wei, A. C. Dillon, *Phy. Rev. B* **2012**, *85*, 035210.
[20] J. S. Hummelshøj, A. C. Luntz, J. K. Nørskov, *J. Chem. Phys.* **2013**, *138*, 034703.
[21] J. Kang, Y. S. Jung, S. H. Wei, A. C. Dillon, *Phys. Rev. B* **2012**, *85*, 035210.
[22] J. M. Garcia-Lastra, J. S. G. Myrdal, R. Christensen, K. S. Thygesen, T. Vegge, *J. Phys. Chem. C* **2013**, *117*, 5568.
[23] M. D. Radin, D. J. Siegel, *Energy Environ. Sci.* **2013**, *6*, 2370.
[24] O. Gerbig, R. Merkle, J. Maier, *Adv. Mater.* **2013**, *25*, 3129.
[25] A. Dunst, V. Epp, I. Hanzu, S. A. Freunberger, M. Wilkening, *Energy Environ. Sci.* **2014**, *7*, 2739.
[26] Q. Sun, Y. Yang, Z.-W. Fu, *Electrochem. Commun.* **2012**, *16*, 22.
[27] P. Hartmann, C. L. Bender, M. Vračar, A. K. Dürr, A. Garsuch, J. Janek, P. Adelhelm, *Nat. Mater.* **2013**, *12*, 228.
[28] X. Ren, Y. Wu, *J. Am. Chem. Soc.* **2013**, *135*, 2923.
[29] ΔG^0 of the reaction $2\ NaO_2 \rightleftharpoons Na_2O_2 + O_2$ amounts to −12 kJ at 300 K and −30 kJ at 600 K. I. Barin, *Thermochemical Data of Pure Substances*, 3rd ed., VCH, Weinheim, **1995**.
[30] C. L. Bender, P. Hartmann, M. Vracar, P. Adelhelm, J. Janek, *Adv. Energy Mater.* **2014**, *4*, 1301863.
[31] S. Y. Kang, Y. Mo, S. P. Ong, G. Ceder, *Nano Lett.* **2014**, *14*, 1016.
[32] O. Gerbig, *Ph.D. Thesis*, University of Stuttgart (Germany) **2014**.
[33] L. Barin, I. Knacke, *Thermochemical Properties of Inorganic Substances*, Springer, Berlin, **1973**.
[34] C. F. Knights, B. A. Philips, *J. Nucl. Mater.* **1979**, *84*, 196.
[35] M. Kim, B. H. Kim, H. C. Choi, B. I. Min, *Phys. Rev. B* **2010**, *81*, 100409.
[36] R. Kovacik, P. Werner, K. Dymkowski, C. Ederer, *Phys. Rev. B* **2012**, *86*, 075130.
[37] S. Riyadi, B. Zhang, R. A. de Groot, A. Caretta, P. H. M. van Loosdrecht, T. T. M. Palstra, G. R. Blake, *Phys. Rev. Lett.* **2012**, *108*, 217206.
[38] J. Fleig, *Solid State Ionics* **2002**, *150*, 181.
[39] R. Hoppe, K.-H. Arend, *Z. Anorg. Allg. Chem.* **1962**, *314*, 4.
[40] A. U. Khan, S. D. Mahanti, *J. Chem. Phys.* **1975**, *63*, 2271.
[41] H. H. Eysel, S. Thym, *Z. Anorg. Allg. Chem.* **1975**, *411*, 97.
[42] This behavior is in contrast to the example of AgCl, where dislocations generated by polishing locally increase the conductvity by 1–2 orders of magnitude at room temperature, but the effects perceptibly degrade over a few hours. J. Fleig, J. Maier, *Ber. Bunsen-Ges.* **1996**, *100*, 607.
[43] R. Merkle, J. Maier, *Phys. Chem. Chem. Phys.* **2002**, *4*, 4140.
[44] J. Maier, *Z. Phys. Chem. (Muenchen, Ger.)* **1984**, *140*, 191.
[45] M. Königstein, *J. Solid State Chem.* **1999**, *147*, 478.
[46] F. A. Kröger, H. J. Vink, in *Solid State Physics, 3: Advances in Research and Applications*, Vol. *3* (Eds: F. Seitz, D. Turnbull), Academic Press, New York **1956**, p. 307.
[47] More precisely, at 175 °C the electrodes are not reversible on the time scale of the impedance measurement (few minutes), while they still allow for equilibration of the samples after a pO_2 change on a time scale of several hours to days at this temperature.
[48] S. Riyadi, S. Giriyapurs, R. A. de Groot, A. Caretta, P. H. M. van Loosdrecht, T. T. M. Palstra, G. R. Blake, *Chem. Mater.* **2011**, *23*, 1578.
[49] G. Brouwer, *Philips Res. Rep.* **1954**, *9*, 366.

© 2015 WILEY-VCH Verlag GmbH & Co. KGaA, Weinheim

[50] In Figure 3 the transition from the pO_2-independent plateau to the sloping region which according to the defect model corresponds to the electroneutrality condition is visible. This indicates a perceptible electron concentration in this region and correspondingly an extremely small hole concentration (band gap ≥ 2 eV).
[51] The transition from the pO_2-independent plateau to the sloping region in Figure 3 is located at $pO_2 = 10^{-2}$–10^{-3} bar, and there holds. Assuming to be in the range of 10^{-6} to 10^{-3} and a band gap of 2 eV ($n \times p \approx 10^{-21}$ at 500 K), the slope of –1 for n in the Brouwer diagram means that the n/p crossing occurs at pO_2 where $n = p = 3 \times 10^{-11}$, i.e., at 10^{1}–10^{5} bar. The zone with perceptible hole conductivity would appear at even larger pO_2.
[52] I. V. Solovyev, Z. V. Pchelkina, V. V. Mazurenko, *CrystEngComm* **2014**, *16*, 522.
[53] M. Kim, B. H. Kim, H. C. Choi, B. I. Min, *Phys. Rev. B* **2010**, *81*, 100409.
[54] R. Kovalcik, P. Werner, K. Dymkowski, C. Ederer, *Phys. Rev. B* **2012**, *86*, 075130.
[55] T. Ishigaki, S. Yamauchi, K. Kishio, J. Mizusaki, K. Fueki, *J. Solid State Chem.* **1988**, *73*, 179.
[56] R. Merkle, J. Maier, *Angew. Chem. Int. Ed.* **2008**, *47*, 3874.
[57] J. Maier, *J. Am. Ceram. Soc.* **1993**, *76*, 1212.
[58] H. J. M. Bouwmeester, C. Song, J. Zhu, J. Yi, M. van Sint Annaland, B. A. Boukamp, *Phys. Chem. Chem. Phys.* **2009**, *11*, 9640.
[59] Strictly speaking this relation holds only for conditions where the $^{32}O_2$ concentration clearly exceeds that of $^{34}O_2$ and $^{36}O_2$, i.e., at sufficiently long times when the gas phase reactant concentration is almost constant (otherwise the gas-phase $^{32}O_2$ concentration gradient would have to be included in the analysis). Further deviations can arise in the analysis of the curve from the fact that $^{36}O_2$ can be formed from dissociative as well as molecular exchange (while $^{34}O_2$ forms only in the dissociative branch, cf. Figure S7, Supporting Information measured for a perovskite for which oxygen incorporation in possible only in atomic form). That the $^{34}O_2$ concentration starts at very low values and passes through a maximum before it decays exponentially comes from the fact that for a fully ^{18}O exchanged sample at the beginning also the dissociative path forms mainly $^{36}O_2$ (due to lack of ^{16}O species in the solid). A more detailed analysis will be given in a following publication.
[60] M. Leonhardt, R. A. De Souza, J. Claus, J. Maier, *J. Electrochem. Soc.* **2002**, *149*, J19.
[61] P. S. Manning, J. D. Sirman, J. A. Kilner, *Solid State Ionics* **1997**, *93*, 125.
[62] C. Y. Yoo, H. J. M. Bouwmeester, *Phys. Chem. Chem. Phys.* **2012**, *14*, 11759.
[63] H. J. M. Bouwmeester, H. Kruidhof, A. J. Burggraaf, *Solid State Ionics* **1994**, *72*, 185.
[64] A. Simon, *Z. Anorg. Allg. Chem.* **1973**, *305*, 301.
[65] Hypothetically, Na might contribute to the ionic conductivity via alkali interstitials. But in order for the 700 ppm Na to have a significant effect, this would require an increase in the Na Frenkel reaction mass action constant over the respective mass action constants for K, Rb or Cs, or a mobility exceeding the respective, and values, by more than 3 orders of magnitude.
[66] M. Bösch, W. Känzig, *Helv. Phys. Acta* **1975**, *48*, 743.
[67] L. S. Leonova, A. V. Levchenko, E. I. Moskvina, N. S. Tkacheva, T. N. Aleshina, S. E. Nadkhina, A. M. Kolesnikova, Yu. A. Dobrovol'skii, N. G. Bukun, *Russ. J. Electrochem.* **2009**, *45*, 593
[68] W. Urland, R. Hoppe, *Z. Anorg. Allg. Chem.* **1972**, *392*, 23.

© 2015 WILEY-VCH Verlag GmbH & Co. KGaA, Weinheim